

Active and silent chromophore isoforms for phytochrome Pr photoisomerization: An alternative evolutionary strategy to optimize photoreaction quantum yields

Yang Yang,^{1,2} Martin Linke,¹ Theodore von Haimberger,¹ Ricardo Matute,³ Leticia González,⁴ Peter Schmieder,⁵ and Karsten Heyne^{1,2,a)}

¹Department of Physics, Freie Universität Berlin, Arnimallee 14, 14195 Berlin, Germany

²Center for Supramolecular Interactions, Takustr. 3, 14195 Berlin, Germany

³Department of Chemistry and Biochemistry, UCLA, 607 Charles E. Young Drive East, Los Angeles, California 90095-1569, USA

⁴Universität Wien, Institut für Theoretische Chemie, Währinger Str. 17, A-1090 Wien

⁵Leibniz-Institut für Molekulare Pharmakologie, Robert-Rössle Str. 10, 13125 Berlin, Germany

(Received 5 November 2013; accepted 11 January 2014; published online 5 February 2014)

Photoisomerization of a protein bound chromophore is the basis of light sensing of many photoreceptors. We tracked Z-to-E photoisomerization of Cph1 phytochrome chromophore PCB in the Pr form in real-time. Two different phycocyanobilin (PCB) ground state geometries with different ring D orientations have been identified. The pre-twisted and hydrogen bonded PCB^a geometry exhibits a time constant of 30 ps and a quantum yield of photoproduct formation of 29%, about six times slower and ten times higher than that for the non-hydrogen bonded PCB^b geometry. This new mechanism of pre-twisting the chromophore by protein-cofactor interaction optimizes yields of slow photoreactions and provides a scaffold for photoreceptor engineering. © 2014 Author(s). All article content, except where otherwise noted, is licensed under a Creative Commons Attribution 3.0 Unported License.

[<http://dx.doi.org/10.1063/1.4865233>]

The photochemical event that initiates light detection in vision, triggering ion transport through membranes and negative phototaxis, is a cis-to-trans or trans-to-cis isomerization of the chromophore, which is part of a photoreceptor. The process is known to occur very quickly with time constant typically between 200 fs and 3 ps for rhodopsin and photoactive yellow protein, respectively. This very fast process is accompanied with a high photoreaction quantum yield typically above 40%, because alternative reaction pathways with slower time constants have a lower probability to occur. Photoisomerization dynamics observed for the photoreceptor phytochrome in its Pr form show longer time constants and a low quantum yield of about 12%, suggesting poor optimization by nature.

Phytochromes¹ are a family of dimeric chromoproteins that absorb light by means of a bound bilin (or linear tetrapyrrole) chromophore, and regulate numerous photoresponses in plants, bacteria, and fungi.^{2–6} They sense red and far-red light by means of two relatively stable conformers: a red light absorbing Pr form with ZZZssa (C₅-Z, C₁₀-Z, C₁₅-Z, C₅-syn, C₁₀-syn, C₁₅-anti, Figure 1) chromophore geometry^{3,4,7–9} and a far-red light absorbing Pfr form with a ZZEssa chromophore conformation.⁴ By photointerconversion between active and inactive forms, phytochromes act as light-regulated master switches for measuring the fluence, direction, and color of the ambient light. Light absorption by the stable Pr conformer triggers an ultrafast Z-to-E isomerization (cis-to-trans) of the C₁₅=C₁₆ methine bridge between the C and D rings of the bilin chromophore accompanied by rotation of ring D.^{10–12} The structural switch, initially localized at the bilin chromophore, is cascaded via intermolecular couplings to slower and widespread structural changes which finally lead to the Pfr form.^{10,13–15} The initial quantum

^{a)} Author to whom correspondence should be addressed. Electronic mail: karsten.heyne@fu-berlin.de

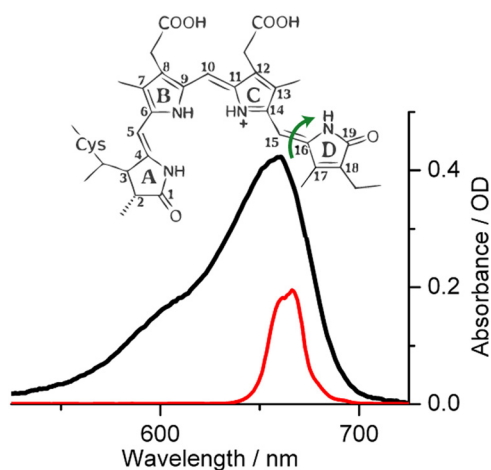


FIG. 1. PCB chromophore of Cph1Δ2 phytochrome with ZZZssa (C_5 - Z , C_{10} - Z , C_{15} - Z , C_5 - syn , C_{10} - syn , C_{15} - $anti$) geometry. Absorption spectrum of Cph1Δ2 Pr form (black line) and applied excitation pulse profile (red line).

yield determines the efficiency, of all successive reaction steps. Therefore, to design synthetic light sensing and light harvesting systems with optimized efficacy it is essential to determine the exact molecular reaction mechanism of ultrafast photoisomerization.

Unfortunately, only a few spectroscopic methods allow direct tracking of fast structural changes in biomolecules on a nanosecond time scale.¹⁶ From direct and indirect methods, it is known that the chromophore in photoreceptors such as rhodopsin, bacteriorhodopsin, and photoactive yellow protein isomerize around a $C=C$ double bond on a time scale of 0.2 to 3 ps with yields of 40% to 65%, a reaction process much faster and five to ten times more efficient in the protein than in solution.^{17–26} The primary photoisomerization of the Pr phytochrome has been investigated by means of ultrafast electronic and vibrational spectroscopy of plant and bacterial phytochromes. From these studies, isomerization time constants in the range of 3 ps to 16 ps and 25 ps to 40 ps were reported,^{14,27–32} followed by lumi-R photoproduct formation with quantum yields in the range of 7% to 16%.^{8,15,28–31}

The low photoproduct quantum yield in phytochrome was proposed to result from photoreceptor heterogeneity.^{33,34} Different geometries of phycocyanobilin (PCB) chromophores in solution were reported with time constants in the range of 3 ps to 500 ps, not detectable in phytochrome Pr photoreaction.^{35,36} Despite the kinetic insight gained from these electronic and vibrational investigations, it was not possible to establish when the $C_{15}=C_{16}$ double bond isomerization and ring D rotation occur, let alone determine the influence of chromophore heterogeneity in phytochromes or the structural orientation of ring D in the photoproduct lumi-R. A nuclear magnetic resonance (NMR) study by Song *et al.*^{34,37} reported two PCB geometries in the Pr ground state Pr-I and Pr-II with different ring D orientations but unknown photoreactive properties. Although traditional femtosecond time resolved infrared and Raman spectroscopic methods provide important information on structural dynamics,^{8,29} they are not able to track orientational changes of vibrational transition dipole moments (tdm) in real time directly.

In this study, we used polarization resolved femtosecond visible pump infrared probe (prfs VIS-IR) spectroscopy^{19,38} to determine the frequency position and orientation of the vibrational modes on a femtosecond time scale from excitation to formation of the first photoproduct lumi-R. Prfs VIS-IR spectroscopy provides direct transient information on the relative angle between the excited electronic transition dipole moment (tdm) and the probed vibrational tdm. The tdm's are fixed within the molecular scaffold of the chromophore, and their properties depend on the electronically excited state. To solely obtain signals from the chromophore's $\nu(C=O)$ and $\nu(C=C)$ stretching vibrations, we used the phycocyanobilin (PCB) chromophore bound to $^{13}C/^{15}N$ labeled Cph1Δ2 protein in D_2O , shifting all $\nu(C=O)$, $\nu(C=C)$, and $\nu(C=N)$ stretching vibrations of the protein to longer wavelengths and all significant protein vibrations out of our spectral window of 1660–1745 cm^{-1} .

Our technique allows us to directly address and answer questions concerning the timing of the chromophore isomerization and ring D rotation, the heterogeneity of chromophore structures and their photoreaction quantum yields, the ZZZssa Pr and the ZZEssa lumi-R ground state geometry (with the help of calculated structures), and the low average quantum yield of the photoreaction compared to that of other photoreceptors. The direct marker bands for Z-to-E isomerization in the 1700 cm^{-1} spectral region were monitored by prfs VIS-IR spectroscopy at a spectral resolution of 1.5 cm^{-1} and a time resolution better than 400 fs, sufficient to resolve sample heterogeneities and dynamics on the time scale believed to govern the S_1 - S_0 transition.

RESULTS AND DISCUSSION

Structural changes initiated by the photoexcitation are reflected in changes in the chromophores' vibrational spectrum. Upon excitation, isotropic transient absorption signals A_{iso} were determined by the absorption signals with parallel A_{\parallel} and perpendicular A_{\perp} polarization, with respect to the pump pulse polarization according to $A_{\text{iso}} = (A_{\parallel} + 2A_{\perp})/3$. All transients were best fitted by a biexponential decay of (4.7 ± 1.4) ps and (30 ± 5) ps.^{8,15,29-31} The error margins represent 1σ standard deviations as determined by exhaustive search analysis (ExSeAn).³⁹

In Figure 2(a), the ground state recovery at 1631 cm^{-1} represents signals of the PCB delocalized mode comprising the $C_{15}=C_{16}$ methine bridge and the $C_{17}=C_{18}$ double bond of the D ring,²⁹ superimposed with signals from ^{13}C labeled carbonyl modes of the protein. Frequencies above 1670 cm^{-1} originate exclusively from chromophore $\nu(\text{C}=\text{O})$ stretching vibrations. The decay of the $\nu(\text{C}_{19}=\text{O})^*$ stretching vibration of ring D in the electronically excited state of Pr (Fig. 2(a)) has its maximum at 1680 cm^{-1} and is red-shifted with respect to its ground state absorption.^{10,27,40} The decay is dominated by the 30 ps time constant (80%). Two distinct bleaching signals of the $\nu(\text{C}_{19}=\text{O})$ stretching vibration in the Pr ground state, at 1701 cm^{-1} and 1708 cm^{-1} , are presented in Figure 2(b). The $\nu(\text{C}_{19}=\text{O}^a)$ bleaching signal at 1701 cm^{-1} has only a negligible 4.7 ps contribution of 5% (Fig. S3(b)),⁴¹ while the $\nu(\text{C}_{19}=\text{O}^b)$ bleaching signal at 1708 cm^{-1} exhibits a pronounced 4.7 ps contribution of 30%. The bleaching recovery at 100 ps is more than seven times greater for $\nu(\text{C}_{19}=\text{O}^b)$ than for $\nu(\text{C}_{19}=\text{O}^a)$.⁴¹ Since the difference between the time constants of the two bleaching bands cannot originate from overlap with

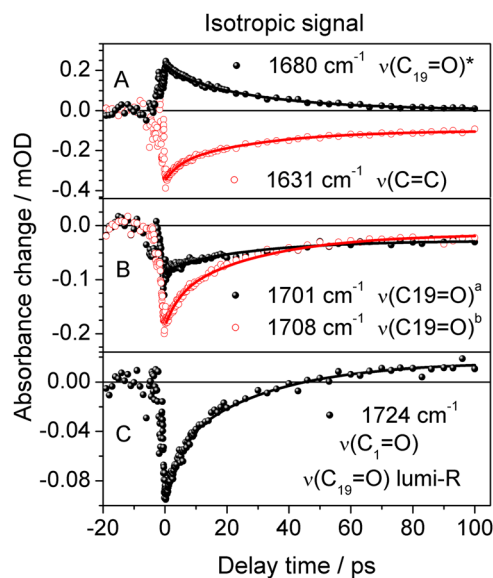


FIG. 2. Transient dynamics at frequency positions of marker bands calculated for isotropic conditions. (a) Bleaching signal of $\nu(\text{C}_{15}=\text{C}_{16})$ and $\nu(\text{C}_{17}=\text{C}_{18})$ stretching vibrations (open red circles), absorption of $\nu(\text{C}_{19}=\text{O})^*$ stretching vibration in the electronically excited state. (b) Bleaching signals of $\nu(\text{C}_{19}=\text{O}^a)$ and $\nu(\text{C}_{19}=\text{O}^b)$ stretching vibrations in the Pr state (solid and open red circles, respectively). (c) Bleaching signal of $\nu(\text{C}_1=\text{O})$ stretching vibration and $\nu(\text{C}_{19}=\text{O})$ absorption of lumi-R.

the $\nu(\text{C}_{19}=\text{O})^*$ vibrational band of Pr, two distinct $\nu(\text{C}_{19}=\text{O})$ vibrations must exist, resulting from at least two different chromophore ground state geometries in Cph1 Δ 2.³⁴ Additional support is given by the analysis of the perturbed free induction decay (PFID) signal.⁴¹ The exponential rise of the PFID signal is related to the Lorentzian line width of the absorption band as its Fourier transform.^{42–44} The optimal fit gives a dephasing time constant of $\tau_{\text{dep}} = 1620$ fs with a 1σ error margin from 1350 fs to 2000 fs (Fig. S1).⁴¹ This translates to a Lorentzian line width range of 6 cm^{-1} to 8 cm^{-1} . Given this line width the bleaching band at $\sim 1705\text{ cm}^{-1}$ in the decay associated spectrum (DAS) at time zero (Fig. 4) cannot be explained by a single absorption band, but can well be simulated with two absorption bands at 1701 cm^{-1} and 1708 cm^{-1} . Exhaustive search analysis of the positions of the two absorption bands shows that their frequencies exhibit distinct values (Fig. S2).⁴¹ Analysis of the polarization resolved DAS (Fig. 4) provides relative angles between the vibrational transition dipole moments of these two vibrations with the electronic transition dipole moment (tdm) of the $S_0 \rightarrow S_1$ transition. We find distinct angles of 29° and 16° for $\nu(\text{C}_{19}=\text{O})^{\text{a}}$ and $\nu(\text{C}_{19}=\text{O})^{\text{b}}$, respectively. The frequency position of the $\nu(\text{C}_{19}=\text{O})$ vibrational band of PCB was reported to be in the spectral region of 1696 cm^{-1} to 1707 cm^{-1} .^{10,27,30,45,46} In previous studies, no direct indications for two $\nu(\text{C}_{19}=\text{O})$ vibrational bands had been reported.²⁹ With our higher spectral resolution of 1.5 cm^{-1} and the time resolved spectroscopic method, we are able to assign two distinct vibrational bands located at 1701 cm^{-1} and 1708 cm^{-1} , each having a width of 8 cm^{-1} . Those frequency positions are known to result from the $\nu(\text{C}_{19}=\text{O})$ stretching vibration in the presence or absence of a hydrogen bond, respectively.¹⁰ However, hot ground states or hot electronic excited states would contribute as positive signals with the same relative angles as the ground state or electronic excited state, respectively.⁴⁷ Hence, neither a hot ground state nor a hot electronic excited state contribution can account for the negative signal at 1701 cm^{-1} with a relative angle of 29° . Additionally, careful analysis of the data show that the second bleaching band signal at 1701 cm^{-1} cannot origin from overlapping of the electronic excited state signal and the ground state bleaching signal (Fig. S8).⁴¹

Thus, these findings demonstrate the heterogeneity of the chromophore structure in phytochromes^{12,14,34,48–51} and shed new light on the analysis of phytochrome infrared spectra in the spectral region around 1700 cm^{-1} .

As it turns out, the crystal structure exhibits only the hydrogen bonded chromophore geometry PCB^a (Fig. 6(a)).¹ Thus, we modeled the second chromophore geometry (Fig. 6(b)), which exhibits a $\nu(\text{C}^{19}=\text{O})^{\text{b}}$ vibrational tdm vector more parallel to the μ_{el} (16°), than the PCB^a geometry (29°). We rotate ring D to the β facial chromophore side and optimized the geometry by density functional theory (DFT). In this position, the $\text{C}_{19}=\text{O}$ group of ring D is not able to form a hydrogen bond. Calculations show a small frequency blue shift of 1 cm^{-1} (Table I), while experiments provide a frequency blue shift of a 7 cm^{-1} . This is due to the missing hydrogen bond of the more planar geometry PCB^b.

TABLE I. Assignment of vibrational modes, their experimental frequencies ν_{exp} , their calculated frequencies ν_{calc} , their experimental angles θ_{exp} relative to the excited electronic tdm, 1σ angle error ranges, calculated angles θ_{calc} relative to the excited electronic tdm. Chromophore geometries are given.

Vibrational mode	ν_{exp} (cm^{-1})	ν_{calc} (cm^{-1})	θ_{exp} ($^\circ$)	1σ ($^\circ$)	θ_{calc} ($^\circ$)	Geom.
Pr $\mu_{\text{C}_{19}=\text{O}}^*$	1680	...	30	27–33	...	ZZZssa
Pr $\mu_{\text{C}_{19}=\text{O}}^{\text{a}}$	1701	1709	29	12–46	21.3	ZZZssa
Pr $\mu_{\text{C}_{19}=\text{O}}^{\text{b}}$	1708	1710	16	6–25 ^a	11.6	ZZZssa
Pr $\mu_{\text{C}_1=\text{O}}^*$	1715	...	60	48–72	...	ZZZssa
Pr $\mu_{\text{C}_1=\text{O}}$	1724	1719	43	36–50	42.4	ZZZssa
Lumi-R $\mu_{\text{C}_{19}=\text{O}}$	1718	1707	54 ^b	46–58	61	ZZEssa

^aError range determined by combination of a covariance method and polarization resolved perturbed free induction decay measurements.

^bLumi-R angle calculated from DAS offset contribution (Fig. S4).⁴¹

At 1724 cm^{-1} , the ground state recovery of the $\nu(\text{C}_1=\text{O})$ vibration of ring A is detected (Fig. 2(c)).^{10,45} Here, we see the strongest contribution of the fast 4.7 ps time constant (40%). The bleaching signal is superimposed with lumi-R photoproduct absorption that arises after 40 ps.^{29,31} Since ring A is not involved in the photoisomerization process, the fast 4.7 ps time constant is attributed to a deactivation pathway.^{27,29,30}

Polarization resolved transients provide information on the angle between the S_0 - S_1 electronic transition dipole moment vector (μ_{el}) and the probed vibrational transition dipole moment vectors (μ_{vib}). As depicted in Figs. 3(a)–3(c), all three bleaching bands exhibit different dichroic ratios (DRs), which are the ratios of parallel and perpendicular absorption signals ($\text{DR} = A_{\parallel}/A_{\perp}$). From the dichroic ratio DR, the angle θ between μ_{el} and μ_{vib} can be calculated as $\theta = \arccos[(2\text{DR} - 1)/(\text{DR} + 2)]^{1/2}$.

Since some of the bleaching transients are partially superimposed on vibrational bands of the electronically excited state, the angles given in Figure 3 provide only a reasonable estimate. A more precise determination can be made from the DAS at time zero. The DAS spectra at time zero for each polarization are presented in Fig. 4. These are derived by biexponential global fits of the transients, and simulated with a sum of five Lorentzian line shapes.⁴¹ The time constants, positions, linewidths, and heights of $\nu(\text{C}=\text{O})$ vibrational bands used for the polarization resolved DAS simulation were obtained by exhaustive search analysis of the complete set of measured data at isotropic polarization, including perturbed free induction decay analysis. The frequency position of the ring A $\nu(\text{C}_1=\text{O})$ vibrational bleaching band is found at 1724 cm^{-1} with a width of 8 cm^{-1} (FWHM).

In the electronically excited state, absorption bands are centered at 1715 cm^{-1} and 1680 cm^{-1} for the $\nu(\text{C}_1=\text{O})^*$ and $\nu(\text{C}_{19}=\text{O})^*$ vibrations, respectively.^{27,30,41} The $\nu(\text{C}_{19}=\text{O})^*$ vibration is most strongly influenced by the electronic excitation and exhibits an absorption line width of 27 cm^{-1} (FWHM) with pronounced transient signals. In contrast, the absorption band

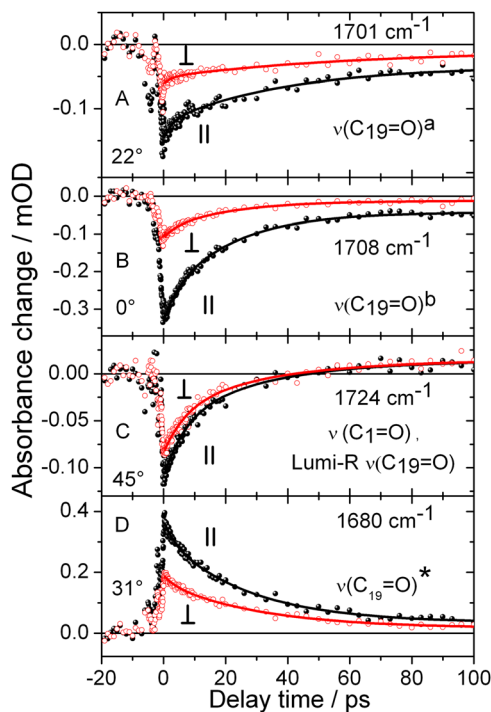


FIG. 3. Polarization resolved transients for parallel (\parallel) and perpendicular (\perp) probe polarization, with respect to the pump pulse polarization. Angles are calculated at a 0.5 ps delay time from the dichroic ratio DR. (a) Ring D $\nu(\text{C}_{19}=\text{O})$ stretch vibration in PCB geometry a; (b) Ring D $\nu(\text{C}_{19}=\text{O})$ stretch vibration in PCB geometry b; (c) Ring A $\nu(\text{C}_1=\text{O})$ stretch vibration and Ring D $\nu(\text{C}_{19}=\text{O})$ stretch vibration of lumi-R; (d) Ring D $\nu(\text{C}_{19}=\text{O})^*$ stretch vibration in the electronically excited state. Reproduced with permission from Yang *et al.*, *J. Am. Chem. Soc.* **134**, 1408–1411 (2012). Copyright 2012 American Chemical Society.

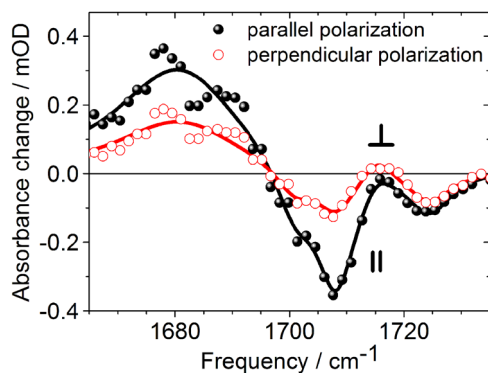


FIG. 4. Decay associated spectrum at time zero and simulation for polarizations parallel (\parallel) and perpendicular (\perp) to the pump pulse polarization. The DAS at time zero is the sum of all DAS components. Negative peak at 1724 cm^{-1} , $\nu(\text{C}_1=\text{O})$ stretching vibration; positive signals around 1715 cm^{-1} , $\nu(\text{C}_1=\text{O})^*$ stretching vibration in the electronically excited state; negative peak at 1708 cm^{-1} , $\nu(\text{C}_{19}=\text{O})^b$ stretching vibration; shoulder at 1701 cm^{-1} , $\nu(\text{C}_{19}=\text{O})^a$ stretching vibration; positive peak at 1680 cm^{-1} , $\nu(\text{C}_{19}=\text{O})^*$ stretching vibration.

of the $\nu(\text{C}_1=\text{O})^*$ vibration exhibits a very small signal and is located at 1715 cm^{-1} with a line width of 8 cm^{-1} FWHM (Fig. S3).⁴¹ The $\nu(\text{C}_1=\text{O})^*$ vibration is only detectable by its dichroic ratio, which is below one and results in a positive peak in the spectrum for perpendicular polarization at around 1715 cm^{-1} (Fig. 4). The small contribution of the $\nu(\text{C}_1=\text{O})^*$ vibration to the signal is attributed to weak anharmonic coupling, which is made possible by negligible structural change in ring A during photoisomerization.²⁹

Analysis of polarization resolved DAS spectra at time zero yields the angles between μ_{el} and the investigated vibrational tdm (Table I). Additionally, the angle (μ_{el} , $\mu_{\text{C}_{19}=\text{O}^*}$) between the S_0 - S_1 tdm and the $\nu(\text{C}_{19}=\text{O})^*$ stretching vibrational tdm was analyzed by ExSeAn and an angle of 30° (1σ range of 18° to 42°) was determined. Error margins given in Table I were derived by the covariance matrix method. All determined angles are compatible with the values directly deduced from the kinetic traces, except the angle (μ_{el} , $\mu_{\text{C}_1=\text{O}^*}$), which is not observable in the transients.

The polarization resolved decay of the $\nu(\text{C}_{19}=\text{O})$ vibration in both its electronically excited state and its ground state is presented in Figs. 5(a) and 5(b) on a logarithmic scale. While the two decaying polarization resolved transients of the $\nu(\text{C}_{19}=\text{O})^b$ bleaching band in Fig. 5(a) show identical slopes, the slopes of the two polarization resolved transients for the $\nu(\text{C}_{19}=\text{O})^*$ stretching band in the electronically excited state are different (Fig. 5(b)). This was interpreted as ring D orientational change in the electronic excited state to the transition state (90° twist) with a time constant of 30 ps and a quantum yield of about 16%.⁵² The time dependent dichroic ratio change (Fig. 5(c)) shows a negligible increase up to 3 ps, followed by a decrease on the time scale of tens of picoseconds. The average angle increases steadily up to 30 ps, supporting the argument that the fast time component of 4.7 ps is associated with C=C bond order reduction, a prerequisite for ring D rotation, and relaxation processes that lead to the initial ground state.^{27,30,31}

Thus, our data support an isomerization mechanism with a single isomerization around the $\text{C}_{15}=\text{C}_{16}$ double bond via a strongly twisted transition state.⁵ An isomerization mechanism including an additional rotation around the $\text{C}_{14}-\text{C}_{15}$ single bond in the electronically excited state would result in negligible dichroic ratio changes and is therefore less likely.^{13,15,53} The initial negligible increase of the dichroic signal (Fig. 5(c)) over time, followed by a delayed dichroic signal decrease can be explained by two models: (I) Ring D rotates away from His290 to smaller twisting angles (clockwise rotation) for PCB^a chromophore geometries with α -facial disposition,² while the non-isomerizing PCB^b chromophores with β -facial disposition rattle around their average orientation. The α -facial disposition is defined by ring D lying on the α -face of the coplanar B- and C-rings.² This implies ring D to be located on the β -facial side after isomerization, in contrast to the Pfr structure reported by Song *et al.*³⁴ on Cph1. (II) A

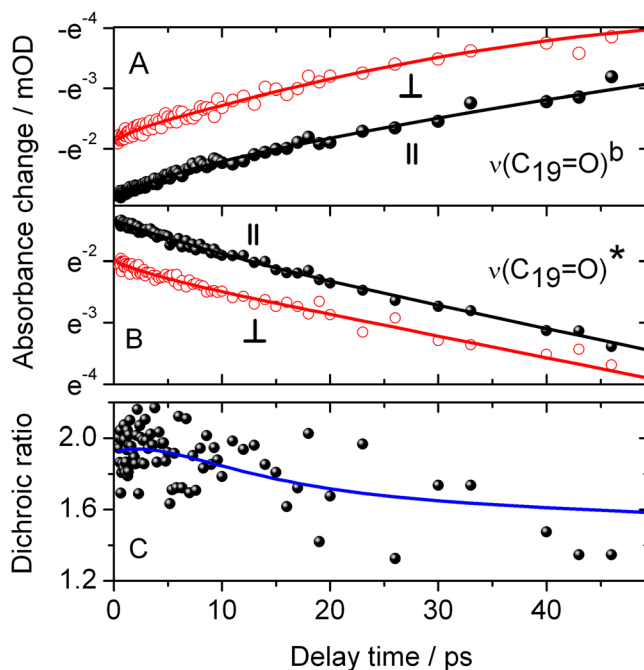


FIG. 5. Polarization resolved transient signals and simulations of the $\nu(\text{C}_{19}=\text{O})$ stretching vibration. (a) $\nu(\text{C}_{19}=\text{O})^{\text{b}}$ vibration in the Pr ground state plotted on a logarithmic scale: Identical slopes for parallel (\parallel) and perpendicular (\perp) polarization indicate no change in dichroic behavior. (b) $\nu(\text{C}_{19}=\text{O})^*$ vibration in the Pr excited state plotted on a logarithmic scale: Transient for parallel polarization (\parallel) exhibits a steeper slope than that for perpendicular (\perp) polarization, demonstrating a change to greater angles. (c) DR calculated by the data (circles) and simulations (blue line) of the $\nu(\text{C}_{19}=\text{O})^*$ vibrational data presented in (b). The simulation shows a negligible increase up to 3 ps, followed by a decrease on the time scale of tens of picoseconds. Reproduced with permission from Yang *et al.*, *J. Am. Chem. Soc.* **134**, 1408–1411 (2012). Copyright 2012 American Chemical Society.

significant part of the PCB^a chromophores with α -facial disposition show counter-clockwise rotation of ring D, thereby slowly passing His290 resulting in a slow dichroic decrease. Another part of PCB^a chromophores with β -facial disposition rotate clockwise to smaller twisting angles on a faster time scale, but do not isomerize, thereby increasing the dichroic ratio (Fig. 5(c)). Non-isomerizing PCB^b chromophores rattle around their average orientation and decay to the ground state. This implies ring D to be located on the α -facial side after isomerization, in agreement with the Pfr structure presented by Song *et al.*³⁴ on Cph1. This is the model we favor.

Combining measured relative angles for the Pr ground state (see Table I) with calculated angles, we are able to verify structural models of the chromophore in the protein binding pocket. The calculated angles of the ZZZssa structural model shown in Fig. 6 are in complete agreement with the experimentally determined ones (Table I).^{1,4} The chromophore structures with orientation of ring D for PCB^a and PCB^b match very well with the Pr-II and Pr-I geometries reported by Song *et al.*,⁵⁴ respectively.

Lumi-R formation was estimated with a quantum yield of about 12% and an angle (μ_{el} , $\mu_{\text{C}_{19}=\text{O}}$) of $\pm 54^\circ$, matching the calculated angle of 61° for the ZZEssa geometry shown in Fig. 6(c) (see also Figs. S4, S6, and S7).⁴¹ From one relative angle alone one cannot determine whether lumi-R adopts a α -facial or β -facial geometry of ring D. Circular dichroism (CD) experiments showed opposite rotational strengths of Pr and Pfr in the longest wavelength band, suggesting a reversal of chirality upon photoisomerization, and thus supporting model II.^{2,55,56} But heterogeneity of Pr ground states complicate interpretation of CD spectra, since PCB^a and PCB^b geometries show opposite rotational strengths with a twofold calculated intensity strength for PCB^a (Fig. S5).⁴¹

Using transients and difference spectra, the individual quantum yields of PCB^a and PCB^b geometries were determined.⁴¹ The more planar PCB^b geometry without hydrogen bonding

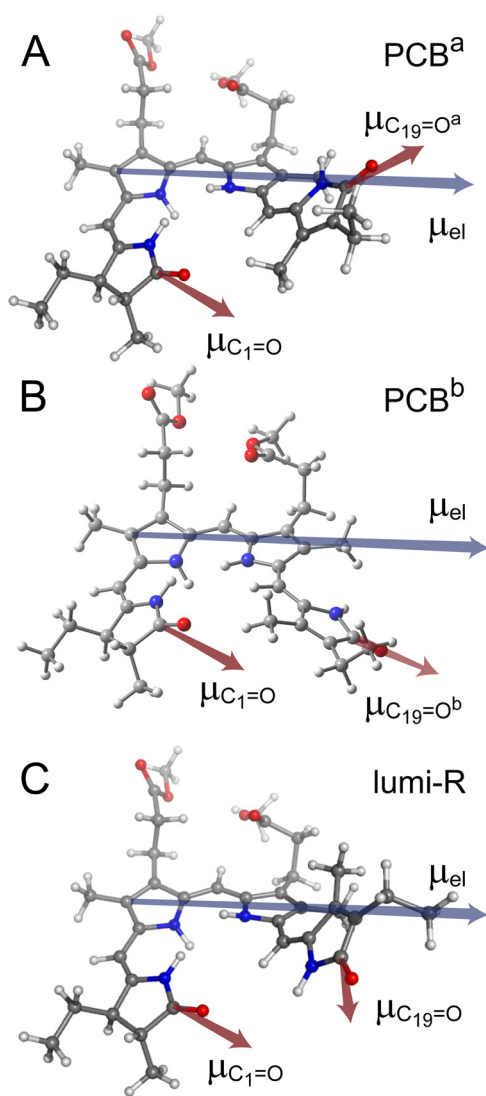


FIG. 6. Calculated PCB chromophore geometries with Pr $S_0 \rightarrow S_1$ transition dipole moment μ_{el} (black arrow) and vibrational tdm's of $\nu(C_{19}=O)^a$ and $\nu(C_1=O)$ (red arrows). μ_{el} and $\mu_{C_1=O}$ show negligible components in the z direction, in contrast to $\mu_{C_{19}=O}^a$. (a) PCB^a geometry, (b) PCB^b geometry, and (c) lumi-R geometry (α -facial ring D position). Note, tdm arrows can point in either direction.

exhibits a ninefold lesser quantum yield of 3%, and has a twofold population as compared to the hydrogen bonded PCB^a geometry with quantum yield of 29%. This indicates that pre-twisting of ring D in the electronic ground state via a single hydrogen bond increases the quantum yield for lumi-R formation significantly.

On the basis of the Cph1 crystal structure,¹ previously reported models,^{12,29,31,32} and our data, we propose a detailed model for counter-clockwise Pr photoisomerization.² Photoexcitation of the chromophore to the electronically excited state S_1 shifts the positive charge from ring B and ring C toward $C_{14}=C_{15}$ methine bridge of ring D. Reduction of negative charge at ring D breaks the hydrogen bond between His290 and the ring D $C_{19}=O$ group.^{12,31} This enables His290 to move away and open the door for counter-clockwise rotation of ring D. Additionally, the positive charge at $C_{14}=C_{15}$ methine bridge alters the hydrogen bond of the water between ring B and ring C, and the hydrogen bond of amino acids Asp207 and Tyr263 in the vicinity of rings C and D. Changes in the hydrogen bond network can induce displacement of Asp207 and Tyr263 reducing steric hindrance for counter-clockwise rotation of

PCB^a ring D with α -facial disposition.^{1,34} Tyr176 is not directly involved in a hydrogen bond network in the Pr state, but is expected to induce steric hindrance for clockwise rotation of PCB^b ring D with β -facial disposition.¹ In the electronically excited state, the double bond character of the C₁₄=C₁₅ methine bridge is reduced, and potential energy from the distorted chromophore ring D is transformed to rotational energy. A part of the PCB^a chromophores passes His290, rotate counter-clockwise to the transition state, and isomerizes, while the remaining PCB^a chromophores rotate clockwise, do not overcome the potential barriers, and relax back to the ground state.

Only about 3% of the chromophores with PCB^b geometry overcome the potential barrier in the electronic excited state and isomerize to lumi-R (Figs. 7(a) and 7(b), blue lines), while 97% relax back to the Pr ground state.

Whether the two Pr isoforms PCB^a and PCB^b undergo interconversion between the silent and the active forms can be tested by temperature dependent measurements.

Rotation of ring D to a more planar geometry is suggested by a dichroic ratio increase in the $\nu(\text{C}_{19}=\text{O})^*$ vibrational band within the first 3 ps (Fig. 5(c)) and a fluorescence red-shift on the same timescale.³¹ A more planar geometry between ring C and ring D reduces the strain in the C₁₄-C₁₅=C₁₆ moiety and induces dramatic changes in the C₁₅-H hydrogen out of plane mode due to increased steric interaction between ring C and ring D within the first picoseconds, as also reported by femtosecond time resolved Raman experiments.²⁹ Intramolecular steric interactions between the C₁₃ methyl of ring C and the N-H of ring D prevent planarity of the C₁₄-C₁₅=C₁₆ moiety, resulting in a barrier in the electronic excited state (Fig. 7).^{14,31,32} In most cases, the rotational energy of the chromophores is too low to pass the potential barrier separating the two geometries. PCB^a chromophores passing His290 experience a shallow excited state potential surface allowing ring D rotation to higher distortion angles and the formation of a transition state in which ring D is twisted by 90°. The increase in distortion angle of ring D is reflected by the decrease in dichroic ratio over time (Fig. 5(c)). After passing the His290, changes in the C₁₅-H hydrogen out of plane mode due to steric interaction between ring C and ring D are negligible.²⁹ As a result of the shallow excited state potential energy surface ring D rotation occurs on a time scale of tens of ps. From there, relaxation to the electronic ground state Pr is observed with the same time constant as lumi-R formation (30 ps).^{29,31,52}

PCB^b chromophores without a hydrogen bond to His290 exhibit a more planar geometry and lower potential energy on the excited state surface as presented in Figure 7, resulting in a lower probability for reaching the transition state and forming lumi-R. As depicted in Figure 7,

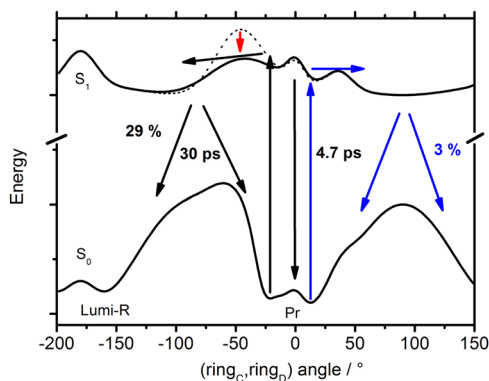


FIG. 7. Schematic potential energy surface as a function of the angle between ring C and ring D plane for model II. Reaction pathways (black arrows) and quantum yields (black numbers) of PCB^a. Time constants are given for both PCB geometries. PCB^b reaction pathways (blue arrows) and quantum yields (blue numbers). Excitation of PCB^b (blue arrow) show small excess energies too low to overcome the barriers efficiently. After PCB^a excitation to the S₁ state (black arrow) the hydrogen bond to His290 breaks and His290 moves away, resulting in a potential barrier reduction (red arrow). The PCB^a chromophores are able to rotate counter-clockwise to the twisted transition state with a -90° distortion angle. With a quantum yield of 29% the forward reaction to lumi-R occurs. Only a small fraction (3%) of the chromophores with PCB^b geometry overcomes the barrier and photoisomerizes to a photoproduct.

the stronger the pre-twisting the higher the potential energy and the higher the lumi-R quantum yield.^{3,4} Consequently, phytochromes with amino acids blocking the space needed for ring D rotation, as shown for the Cph1-Y263F mutant,⁶⁰ or in which ring D is fixed with additional hydrogen bonds, would exhibit a reduced quantum yield for lumi-R formation. Such observations have been reported by other groups, thus corroborating our model.^{27,28,53,57,60}

CONCLUSION

In Cph1 phytochrome, Pr photoisomerization and rotation of ring D occurs in the electronic excited state via a 90° twisted transition state with a time constant of 30 ± 5 ps. A sixfold faster relaxation time constant of 4.7 ± 1.4 ps is also present. This would normally lead to a poor quantum yield. However, heterogeneity, that is, two possible chromophore geometries PCB^a and PCB^b, leads to two photoreactions with differing efficiencies. We identified PCB^a and PCB^b geometries with distinct quantum yields of 29% and 3%, respectively. The PCB^a and PCB^b geometries match the Pr-II and Pr-I geometries determined by NMR studies, respectively.³⁷ PCB^a (Pr-II) has a strongly pre-twisted ring D geometry induced by a hydrogen bond between ring D's carbonyl group and His290. The pre-twisting of PCB^a (Pr-II) allows a higher potential energy in the electronic excited state to be reached, permitting potential barriers induced by steric hindrance to be overcome. This chromophore geometry exhibits a ninefold higher quantum yield than PCB^b (Pr-I), but a sixfold longer time constant of 30 ± 5 ps. The high quantum yield in combination with a long time constant is very unusual for photoreceptors.

This demonstrates an alternative evolutionary strategy to improve photoreactions. Pre-twisting of the chromophore by strong steric interactions and hydrogen bonding in the ground and electronic excited states enhance the photoreaction quantum yield by separating reaction pathways for differing geometries in the electronic excited state. This mechanism optimizes yields of slow photoreactions by large structural rearrangements and provides a scaffold for photoreceptor engineering.

METHODS

Pump and probe pulses were generated using nonlinear optical methods. By difference frequency mixing in various steps, we obtained mid-IR pulses of 200 fs (FWHM) or shorter at a repetition rate of 1.088 kHz. Simultaneously, laser pulses of 200 fs duration at 660 nm were generated and used to photoexcite the sample in the absorption maximum of the Pr form, thus initiating the photoreaction (Fig. 1). Photoselection experiments were performed using focal pump pulse diameters of 500 μm , sample thicknesses of 50 μm , focal probe pulse diameters of 180 μm , and pump pulse energies of 30 nJ. This results in excitation coefficients of below 3% and in relative signal strengths in agreement with electronic extinction coefficient of PCB ($\sim 82\,000$ (Mcm)⁻¹) and extinction coefficient of C=O stretching vibrations (~ 2000 (Mcm)⁻¹). The transient absorption was simultaneously probed by two mid-IR pulses with polarizations oriented parallel and perpendicular, with respect to the pump pulse polarization at various delay times.⁴⁷ Probe pulses were dispersed with an imaging spectrograph and recorded with a 2×32 element MCT array detector. We prepared the ¹³C/¹⁵N labeled Cph1 Δ 2 phytochrome holoprotein (non-labelled PCB chromophore) in ²H₂O solution at an optical density of 0.4 optical density at 660 nm, as described previously.^{9,41,43,48,51,58,59} Background illumination at wavelengths longer than 715 nm ensures that the sample remains in the Pr form. The high repetition rate requires that the sample be moved across the focused laser beams with a Lissajous sample cell in order to avoid multiple excitation of a specific sample volume. For comparison, the vibrational tdm's were determined theoretically at the B3LYP/6-31G(d) level of theory. The structures of the different chromophores were obtained as described.⁴¹

ACKNOWLEDGMENTS

This work was supported by the Deutsche Forschungsgemeinschaft (SFB 1078, TP B3). We thank MPI-Halle and the Computing Center at the FUB (ZEDAT) for support.

- ¹L. O. Essen, J. Mailliet, and J. Hughes, "The structure of a complete phytochrome sensory module in the Pr ground state," *Proc. Natl. Acad. Sci. U.S.A.* **105**, 14709–14714 (2008).
- ²N. C. Rockwell, L. Shang, S. S. Martin, and J. C. Lagarias, "Distinct classes of red/far-red photochemistry within the phytochrome superfamily," *Proc. Natl. Acad. Sci. U.S.A.* **106**, 6123–6127 (2009).
- ³J. R. Wagner, J. S. Brunzelle, K. T. Forest, and R. D. Vierstra, "A light-sensing knot revealed by the structure of the chromophore-binding domain of phytochrome," *Nature* **438**, 325–331 (2005).
- ⁴J. Hughes, "Phytochrome three-dimensional structures and functions," *Biochem. Soc. Trans.* **38**, 710–716 (2010).
- ⁵N. C. Rockwell, Y. S. Su, and J. C. Lagarias, "Phytochrome structure and signaling mechanisms," *Annu. Rev. Plant Biol.* **57**, 837–858 (2006).
- ⁶N. C. Rockwell and J. C. Lagarias, "The structure of phytochrome: A picture is worth a thousand spectra," *Plant Cell* **18**, 4–14 (2006).
- ⁷R. A. Matute, R. Contreras, G. Pérez-Hernández, and L. González, "The chromophore structure of the cyanobacterial phytochrome Cph1 as predicted by time-dependent density functional theory," *J. Phys. Chem. B* **112**, 16253–16256 (2008).
- ⁸J. J. van Thor, K. L. Ronayne, and M. Towrie, "Formation of the early photoproduct Lumi-R of cyanobacterial phytochrome Cph1 observed by ultrafast mid-infrared spectroscopy," *J. Am. Chem. Soc.* **129**, 126–132 (2007).
- ⁹J. Hahn, H. M. Strauss, and P. Schmieder, "Heteronuclear NMR investigation on the structure and dynamics of the chromophore binding pocket of the cyanobacterial phytochrome Cph1," *J. Am. Chem. Soc.* **130**, 11170–11178 (2008).
- ¹⁰H. Foersterdorf, C. Benda, W. Gartner, M. Storf, H. Scheer, and F. Siebert, "FTIR studies of phytochrome photoreactions reveal the C=O bands of the chromophore: Consequences for its protonation states, conformation, and protein interaction," *Biochemistry* **40**, 14952–14959 (2001).
- ¹¹F. Siebert, R. Grimm, W. Rudiger, G. Schmidt, and H. Scheer, "Infrared-spectroscopy of phytochrome and model pigments," *Eur. J. Biochem.* **194**, 921–928 (1990).
- ¹²K. Heyne, J. Herbst, D. Stehlik, B. Esteban, T. Lamparter, J. Hughes, and R. Diller, "Ultrafast dynamics of phytochrome from the cyanobacterium *Synechocystis*, reconstituted with phycocyanobilin and phycoerythrobilin," *Biophys. J.* **82**, 1004–1016 (2002).
- ¹³J. Matysik, P. Hildebrandt, W. Schlamann, S. E. Braslavsky, and K. Schaffner, "Fourier-transform resonance Raman-spectroscopy of intermediates of the phytochrome photocycle," *Biochemistry* **34**, 10497–10507 (1995).
- ¹⁴V. A. Sineshchekov, "Photobiophysics and photobiochemistry of the heterogeneous phytochrome system," *Bba-Bioenergetics* **1228**, 125–164 (1995).
- ¹⁵F. Andel, K. C. Hasson, F. Gai, P. A. Anfinrud, and R. A. Mathies, "Femtosecond time-resolved spectroscopy of the primary photochemistry of phytochrome," *Biospectroscopy* **3**, 421–433 (1997).
- ¹⁶H. Ihee, S. Rajagopal, V. Srajer, R. Pahl, S. Anderson, M. Schmidt, F. Schotte, P. A. Anfinrud, M. Wulff, and K. Moffat, "Visualizing reaction pathways in photoactive yellow protein from nanoseconds to seconds," *Proc. Natl. Acad. Sci. U.S.A.* **102**, 7145–7150 (2005).
- ¹⁷D. Polli, P. Altoe, O. Weingart, K. M. Spillane, C. Manzoni, D. Brida, G. Tomasello, G. Orlandi, P. Kukura, R. A. Mathies, M. Garavelli, and G. Cerullo, "Conical intersection dynamics of the primary photoisomerization event in vision," *Nature* **467**, 440–443 (2010).
- ¹⁸J. Herbst, K. Heyne, and R. Diller, "Femtosecond infrared spectroscopy of bacteriorhodopsin chromophore isomerization," *Science* **297**, 822–825 (2002).
- ¹⁹K. Heyne, O. F. Mohammed, A. Usman, J. Dreyer, E. T. J. Nibbering, and M. A. Cusanovich, "Structural evolution of the chromophore in the primary stages of trans/cis isomerization in photoactive yellow protein," *J. Am. Chem. Soc.* **127**, 18100–18106 (2005).
- ²⁰A. Usman, O. F. Mohammed, K. Heyne, J. Dreyer, and E. T. J. Nibbering, "Excited state dynamics of a PYP chromophore model system explored with ultrafast infrared spectroscopy," *Chem. Phys. Lett.* **401**, 157–163 (2005).
- ²¹K. Heyne, J. Herbst, B. Dominguez-Herradon, U. Alexiev, and R. Diller, "Reaction control in bacteriorhodopsin: Impact of arg82 and asp85 on the fast retinal isomerization, studied in the second site revertant arg82ala/gly231cys and various purple and blue forms of bacteriorhodopsin," *J. Phys. Chem. B* **104**, 6053–6058 (2000).
- ²²P. Hamm, M. Zurek, T. Roschinger, H. Patzelt, D. Oesterheld, and W. Zinth, "Femtosecond spectroscopy of the photoisomerisation of the protonated Schiff base of all-trans retinal," *Chem. Phys. Lett.* **263**, 613–621 (1996).
- ²³S. Schenkl, F. van Mourik, G. van der Zwan, S. Haacke, and M. Chergui, "Probing the ultrafast charge translocation of photoexcited retinal in bacteriorhodopsin," *Science* **309**, 917–920 (2005).
- ²⁴Q. Wang, R. W. Schoenlein, L. A. Peteanu, R. A. Mathies, and C. V. Shank, "Vibrationally coherent photochemistry in the femtosecond primary event of vision," *Science* **266**, 422–424 (1994).
- ²⁵J. Döbler, W. Zinth, W. Kaiser, and D. Oesterheld, "Excited-state reaction dynamics of bacteriorhodopsin studied by femtosecond spectroscopy," *Chem. Phys. Lett.* **144**, 215–220 (1988).
- ²⁶H. Kandori, Y. Shichida, and T. Yoshizawa, "Photoisomerization in rhodopsin," *Biochemistry-Moscow+* **66**, 1197–1209 (2001).
- ²⁷K. C. Toh, E. A. Stojkovic, A. B. Rupenyan, I. H. M. van Stokkum, M. Salumbides, M.-L. Groot, K. Moffat, and J. T. M. Kennis, "Primary reactions of bacteriophytochrome observed with ultrafast mid-infrared spectroscopy," *J. Phys. Chem. A* **115**, 3778–3786 (2011).
- ²⁸K. C. Toh, E. A. Stojkovic, I. H. M. van Stokkum, K. Moffat, and J. T. M. Kennis, "Proton-transfer and hydrogen-bond interactions determine fluorescence quantum yield and photochemical efficiency of bacteriophytochrome," *Proc. Natl. Acad. Sci. U.S.A.* **107**, 9170–9175 (2010).
- ²⁹J. Dasgupta, R. R. Frontiera, K. C. Taylor, J. C. Lagarias, and R. A. Mathies, "Ultrafast excited-state isomerization in phytochrome revealed by femtosecond stimulated Raman spectroscopy," *Proc. Natl. Acad. Sci. U.S.A.* **106**, 1784–1789 (2009).
- ³⁰C. Schumann, R. Gross, N. Michael, T. Lamparter, and R. Dillier, "Sub-picosecond mid-infrared spectroscopy of phytochrome Agp1 from *Agrobacterium tumefaciens*," *Chemphyschem* **8**, 1657–1663 (2007).
- ³¹M. G. Müller, I. Lindner, I. Martin, W. Gartner, and A. R. Holzwarth, "Femtosecond kinetics of photoconversion of the higher plant photoreceptor phytochrome carrying native and modified chromophores," *Biophys. J.* **94**, 4370–4382 (2008).

- ³²A. R. Holzwarth, E. Venuti, S. E. Braslavsky, and K. Schaffner, "The phototransformation process in phytochrome. 1. Ultrafast fluorescence component and kinetic-models for the initial Pr-JPfr transformation steps in native phytochrome," *Biochim. Biophys. Acta* **1140**, 59–68 (1992).
- ³³H. Kandori, K. Yoshihara, and S. Tokutomi, "Primary process of phytochrome—Initial step of photomorphogenesis in green plants," *J. Am. Chem. Soc.* **114**, 10958–10959 (1992).
- ³⁴C. Song, G. Psakis, K. Langlois, J. Mailliet, W. Gärtner, J. Hughes, and J. Matysik, "Two ground state isoforms and a chromophore D-ring photoflip triggering extensive intramolecular changes in a canonical phytochrome," *Proc. Natl. Acad. Sci. U.S.A.* **108**, 3842–3847 (2011).
- ³⁵A. H. Goller, D. Strehlow, and G. Hermann, "The excited-state chemistry of phycocyanobilin: A semiempirical study," *Chemphyschem* **6**, 1259–1268 (2005).
- ³⁶M. Bischoff, G. Hermann, S. Rentsch, D. Strehlow, S. Winter, and H. Chosrowjan, "Excited-state processes in phycocyanobilin studied by femtosecond spectroscopy," *J. Phys. Chem. B* **104**, 1810–1816 (2000).
- ³⁷C. Song, T. Rohmer, M. Tiersch, J. Zaanen, J. Hughes, and J. Matysik, "Solid-state NMR spectroscopy to probe photoactivation in canonical phytochromes," *Photochem. Photobiol.* **89**, 259–273 (2013).
- ³⁸M. Lim, T. A. Jackson, and P. A. Anfinrud, "Binding of CO to myoglobin from a heme pocket docking site to form nearly linear Fe-C-O," *Science* **269**, 962–966 (1995).
- ³⁹T. A. Roelofs, C. H. Lee, and A. R. Holzwarth, "Global target analysis of picosecond chlorophyll fluorescence kinetics from pea-chloroplasts—A new approach to the characterization of the primary processes in photosystem-II alpha-units and beta-units," *Biophys. J.* **61**, 1147–1163 (1992).
- ⁴⁰M. Theisen, M. Linke, M. Kerbs, H. Fidder, A. Madjet Mel, A. Zacarias, and K. Heyne, "Femtosecond polarization resolved spectroscopy: A tool for determination of the three-dimensional orientation of electronic transition dipole moments and identification of configurational isomers," *J. Chem. Phys.* **131**, 124511 (2009).
- ⁴¹See supplementary material at <http://dx.doi.org/10.1063/1.4865233> for materials and methods, computational details, PFID analysis, analysis of spectral components, CD spectra, and Lumi-R quantum yield.
- ⁴²P. Hamm, "Coherent effects in femtosecond infrared-spectroscopy," *Chem. Phys.* **200**, 415–429 (1995).
- ⁴³K. Wynne and R. M. Hochstrasser, "The theory of ultrafast vibrational spectroscopy," *Chem. Phys.* **193**, 211–236 (1995).
- ⁴⁴P. Nuernberger, K. F. Lee, A. Bonvalet, T. Polack, M. H. Vos, A. Alexandrou, and M. Joffre, "Suppression of perturbed free-induction decay and noise in experimental ultrafast pump-probe data," *Opt. Lett.* **34**, 3226–3228 (2009).
- ⁴⁵J. J. van Thor, N. Fisher, and P. R. Rich, "Assignments of the Pfr-Pr FTIR difference spectrum of cyanobacterial phytochrome Cph1 using N-15 and C-13 isotopically labeled phycocyanobilin chromophore," *J. Phys. Chem. B* **109**, 20597–20604 (2005).
- ⁴⁶H. Foerstendorf, T. Lamparter, J. Hughes, W. Gärtner, and F. Siebert, "The photoreactions of recombinant phytochrome from the cyanobacterium *Synechocystis*: A low-temperature UV-Vis and FT-IR spectroscopic study," *Photochem. Photobiol.* **71**, 655–661 (2000).
- ⁴⁷M. Linke, Y. Yang, B. Zienicke, M. A. S. Hammam, T. Von Haimberger, A. Zacarias, K. Inomata, T. Lamparter, and K. Heyne, "Electronic transitions and heterogeneity of the bacteriophytochrome Pr absorption band: An angle balanced polarization resolved femtosecond VIS pump-IR probe study," *Biophys. J.* **105**, 1756–1766 (2013).
- ⁴⁸M. H. Lim, T. A. Jackson, and P. A. Anfinrud, "Femtosecond near-IR absorbance study of photoexcited myoglobin: Dynamics of electronic and thermal relaxation," *J. Phys. Chem.-US* **100**, 12043–12051 (1996).
- ⁴⁹D. von Stetten, M. Gunther, P. Scheerer, D. H. Murgida, M. A. Mroginski, N. Krauss, T. Lamparter, J. Zhang, D. M. Anstrom, R. D. Vierstra, K. T. Forest, and P. Hildebrandt, "Chromophore heterogeneity and photoconversion in phytochrome crystals and solution studied by resonance Raman spectroscopy," *Angew Chem. Int. Ed. Engl.* **47**, 4753–4755 (2008).
- ⁵⁰V. Sineshchekov, A. Loskovich, N. Inagaki, and M. Takano, "Two native pools of phytochrome A in monocots: Evidence from fluorescence investigations of phytochrome mutants of rice," *Photochem. Photobiol.* **82**, 1116–1122 (2006).
- ⁵¹M. Roben, J. Hahn, E. Klein, T. Lamparter, G. Psakis, J. Hughes, and P. Schmieder, "NMR spectroscopic investigation of mobility and hydrogen bonding of the chromophore in the binding pocket of phytochrome proteins," *Chemphyschem* **11**, 1248–1257 (2010).
- ⁵²K. Heyne and T. Rubin, *Messvorrichtung und Verfahren zur Untersuchung eines Probegases mittels Infrarot-Absorptionsspektroskopie* (H. GmbH, Germany, 2009).
- ⁵³A. J. Fischer and J. C. Lagarias, "Harnessing phytochrome's glowing potential," *Proc. Natl. Acad. Sci. U.S.A.* **101**, 17334–17339 (2004).
- ⁵⁴K. Heyne, M. Hartmann, and K. Molkenhuth, *Pulsshaper und Laser mit Pulsshaper* (F. U. Berlin, Germany, 2008).
- ⁵⁵B. Borucki, H. Otto, G. Rottwinkel, J. Hughes, M. P. Heyn, and T. Lamparter, "Mechanism of Cph1 phytochrome assembly from stopped-flow kinetics and circular dichroism," *Biochemistry* **42**, 13684–13697 (2003).
- ⁵⁶S. C. Björling, C.-F. Zhang, D. L. Farrens, P. S. Song, and D. S. Kliger, "Time-resolved circular dichroism of native oat phytochrome photointermediates," *J. Am. Chem. Soc.* **114**, 4581–4588 (1992).
- ⁵⁷X. Yang, J. Kuk, and K. Moffat, "Conformational differences between the Pfr and Pr states in *Pseudomonas aeruginosa* bacteriophytochrome," *Proc. Natl. Acad. Sci. U.S.A.* **106**, 15639–15644 (2009).
- ⁵⁸H. M. Strauss, J. Hughes, and P. Schmieder, "Heteronuclear solution-state NMR studies of the chromophore in cyanobacterial phytochrome Cph1," *Biochemistry* **44**, 8244–8250 (2005).
- ⁵⁹M. H. Lim, T. A. Jackson, and P. A. Anfinrud, "Modulating carbon monoxide binding affinity and kinetics in myoglobin: The roles of the distal histidine and the heme pocket docking site," *J. Biol. Inorg. Chem.* **2**, 531–536 (1997).
- ⁶⁰J. Mailliet, G. Psakis, K. Feilke, V. Sineshchekov, L.-O. Essen, and J. Hughes, "Spectroscopy and a high-resolution crystal structure of Tyr263 mutants of cyanobacterial phytochrome Cph1," *J. Mol. Biol.* **413**, 115–127 (2011).